Aerosol and Air Quality Research, 17: 3079–3090, 2017

ISSN: 1680-8584 print / 2071-1409 online
doi: 10.4209/aaqr.2016.12.0592

Model Estimation of Sulfate Aerosol Sources Collected at Cape Hedo during an Intensive Campaign in October–November, 2015

Syuichi Itahashi[1*], Shiro Hatakeyama[2,3,4], Kojiro Shimada[2,3†], Shiori Tatsuta[3], Yuta Taniguchi[3], Chak K. Chan[5], Yong Pyo Kim[2,6,7], Neng-Huei Lin[2,8], Akinori Takami[9]

[1] *Environmental Science Research Laboratory, Central Research Institute of Electric Power Industry, Abiko, Chiba 270-1194, Japan*
[2] *Global Innovation Research Organization, Tokyo University of Agriculture and Technology, Fuchu, Tokyo 183-8509, Japan*
[3] *Graduate School of Agriculture, Tokyo University of Agriculture and Technology, Fuchu, Tokyo 183-8509, Japan*
[4] *Center for Environmental Science in Saitama, Kazo, Saitama 347-0115, Japan*
[5] *School of Energy and Environment, City University of Hong Kong, Kowloon, Hong Kong, China*
[6] *Department of Chemical, Engineering & Materials Science, Ewha Womans University, Seodaemun-gu, Seoul 120-750, Korea*
[7] *Department of Environmental Science and Engineering, Ewha Womans University, Seodaemun-gu, Seoul 120-750, Korea*
[8] *Department of Atmospheric Sciences, National Central University, Chung-Li 32001, Taiwan*
[9] *National Institute for Environmental Studies, Tsukuba, Ibaraki 305-8506, Japan*

ABSTRACT

An intensive observation campaign at Cape Hedo, Okinawa, Japan was conducted from late October to early November 2015 to investigate the behavior of long-range transported atmospheric pollutants. During this period, sulfate (SO_4^{2-}) was the dominant aerosol component. The sources of SO_4^{2-} were estimated by using the air quality model with the tagged tracer method. The main source of high SO_4^{2-} concentration varied day-to-day. When the westerly wind was dominant (October 27), the main source was anthropogenic SO_2 emissions in China. When the northerly wind prevailed (November 1), the impact of volcanoes in western Japan was significant and the conversion ratio from SO_2 to SO_4^{2-} was lowest, at less than 70%, because of the faster transport. During the latter part of the campaign, the northerly to easterly winds were prominent, and the impacts of Korea, Japan, and ships on SO_4^{2-} observed at Cape Hedo were also clear. When the contributions from Korea, Japan, and ships were the highest (November 4), the conversion ratio was also the highest, at greater than 95% because of long-range transport. The modeled sources of volcanoes and ship emissions corresponded well with the observed coarse-mode SO_4^{2-} and V/Mn ratio, respectively. The mutual evaluation of sources from model and observations enable SO_4^{2-} sources to be estimated with higher confidence.

Keywords: Air quality model; Source apportionment; Tagged tracer method; East Asia.

INTRODUCTION

Air quality in Asia is a major regional-to-global environmental problem (Carmichael *et al.*, 2009). China is a particularly important source region because Chinese anthropogenic emissions account for a major proportion of global emissions (Janssens-Maenhout *et al.*, 2015). Several collaborative international experiments have been performed over the western Pacific region (e.g., Nakajima *et al.*, 2007). Investigating the transformation of aerosols during long-range transport (LRT) is essential for understanding atmospheric pollution impact and regional climate change.

During late October to early November, 2015, an intensive observation campaign was conducted at Cape Hedo Atmosphere and Aerosol Monitoring Station (CHAAMS), Okinawa, Japan (Fig. 1). CHAAMS is located in northern Okinawa (26.87°N, 128.25°E, 60 m above sea level), far from Naha City, which is the largest city on Okinawa. The location of CHAAMS is suitable for capturing the atmospheric pollutants via LRT, and has already revealed the behavior of aerosols affected by the LRT (Takami *et al.*, 2007; Takiguchi *et al.*, 2008; Hatakeyama *et al.*, 2011; Shimada *et al.*, 2015). During the intensive observation

† Now at School of Creative Science and Engineering, Waseda University, Shinjuku, Tokyo 169-8555, Japan.

* Corresponding author.
Tel.: 81-70-5080-1394; Fax: 81-4-7183-2966
E-mail address: isyuichi@criepi.denken.or.jp

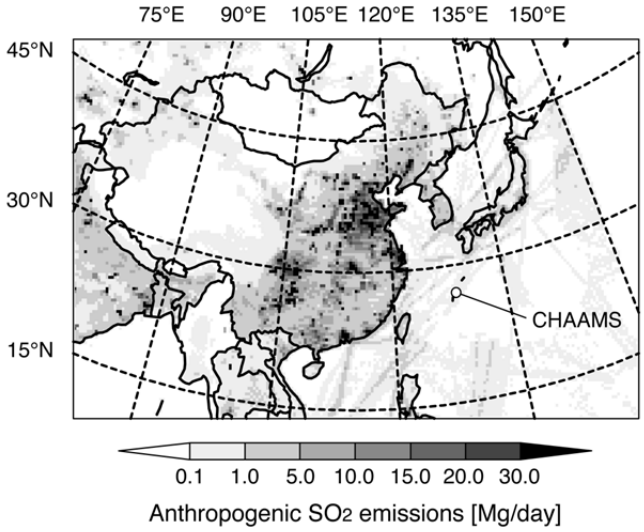

Fig. 1. Modeling domain with anthropogenic SO_2 emissions used in this study. The open circle indicates the location of CHAAMS.

campaign in 2015 and other seasonal campaigns at CHAMMS, sulfate aerosol (SO_4^{2-}), which is mainly produced by the oxidation of sulfur dioxide (SO_2), was the dominant aerosol component at CHAAMS (Tatsuta *et al.*, 2017).

SO_4^{2-} is generally present in particulate matter with aerodynamic diameters of less than 2.5 μm ($PM_{2.5}$), an important aerosol component in Asia (Zhang *et al.*, 2007). Because of the long lifetime of SO_4^{2-} in the atmosphere, LRT is likely to have a major effect in downwind regions. Comparing these results with observations over a metropolitan area and a remote island in western Japan indicated that SO_4^{2-} mainly came from LRT (Kaneyasu *et al.*, 2014). A large longitudinal gradient of SO_4^{2-}, with higher concentrations over western Japan and lower concentrations over eastern Japan, was revealed by the compiled dataset of the observation network over Japan (Aikawa *et al.*, 2010). In addition to the ground-based observations, satellite observations of aerosol optical depth, mainly arising from SO_4^{2-}, also indicated a longitudinal gradient over adjacent oceans in East Asia (Itahashi *et al.*, 2012a). These observations highlighted the importance of the LRT from continental Asia to downwind regions of Japan.

An air quality model can provide valuable insights for evaluating the impact of the LRT, especially for quantitative assessment. The traditional approach of sensitivity analysis, in which one model parameter (e.g., emissions from a specific source) is tested at a time, has been widely used to estimate sources. One of the limitations of sensitivity analysis is the computational burden of testing many model parameters. The decoupled direct method has been used to perform sophisticated sensitivity analysis of SO_4^{2-} sources in East Asia (Itahashi *et al.*, 2012b); however, this method is also computationally intensive. Higher computational efficiency has allowed the tagged tracer method to be used to estimate year-round source apportionment of SO_4^{2-} over East Asia (Itahashi *et al.*, 2017a). The LRT from mainland China was found to have a large impact over downwind regions of Taiwan, Korea, and Japan throughout 2005, when the anthropogenic SO_2 emissions from China peaked. However, this previous study was not focused on the source impact at Okinawa and the source assessment was based on a monthly to annually averaged time scale; thus, the work did not examine detailed transport patterns.

In the present work, we evaluated the sources of SO_4^{2-} by the tagged tracer method on a daily averaged time scale based on the model evaluation in comparison with intensive observations. Model estimated sources were compared with observed indicators to improve our evaluation of the sources of SO_4^{2-}. To the best of our knowledge, this is the first mutual source evaluation of SO_4^{2-} between the tagged tracer method with the air quality model and observed indicators. To exclude the effect of sea salt, non-sea salt SO_4^{2-} (nss-SO_4^{2-}) was analyzed throughout this study. The concentration of non-sea salt SO_4^{2-} (units of micrograms per cubic meter) was calculated from the following equation by the conservative assumption of Na as a sea salt tracer. For simplicity, we refer to nss-SO_4^{2-} as SO_4^{2-} hereafter.

$$\text{nss-}SO_4^{2-} = SO_4^{2-} - 0.251 \times Na^+. \quad (1)$$

METHODS

Observations

During the intensive observation campaign at CHAAMS, 24 h sampling starting from 10:00 local time (LT) to 10:00 the next day was conducted from October 26 to November 8, 2015 (13 samples in total). $PM_{2.5}$ concentrations were analyzed based on the following two observation methods. $PM_{2.5}$ was sampled with a high-volume air sampler at a flow rate of 740 L min^{-1} by using a $PM_{2.5}$ impactor developed by Kaneyasu (2010). Atmospheric aerosols were sampled with a cascade impactor (Model 3180, KANOMAX) with a flow rate of 40 L min^{-1} and segregated into six size bins according to particle diameter (D_p): D_p > 10 μm; 10 μm ≥ D_p > 2.5 μm; 2.5 μm ≥ D_p > 1 μm; 1 μm ≥ D_p > 0.5 μm; 0.5 μm ≥ D_p > 0.1 μm; and 0.1 μm ≥ D_p. The samples were

collected on a Teflon (PTFE) filter, and cut into two pieces for analyzing ions and metals. The ions in the aerosols were analyzed by ion chromatography and metals were analyzed by inductively coupled plasma-mass spectrometry. The observation details of ions and metals conducted on CHAAMS are reported in the companion articles (Tatsuta *et al.*, 2017; Taniguchi *et al.*, 2017).

Air Quality Model Simulation

To conduct the model simulation, we used the regional chemical transport model of the Comprehensive Air Quality Model with Extensions (CAMx) version 6.11 (ENVIRON International Corporation, 2014). CAMx was configured with a 36-km horizontal resolution and 220 × 140 grid points, centered at 35°N and 115°E on a Lambert conformal projection, covering East Asia (Fig. 1). For the vertical resolution, 37 non-uniformly spaced layers from the surface to 50 hPa were used. CAMx was driven by the meteorological fields calculated by the Weather Research and Forecasting model version 3.6.1 (Skamarock *et al.*, 2008). We have previously used the CAMx model to study the behavior of air pollutants (e.g., ozone, SO_4^{2-}) over East Asia (Itahashi *et al.*, 2015; 2017a). The lateral boundary conditions were prepared from the global chemical transport of MOZART-4 (Emmons *et al.*, 2010). The model calculation started from October 20 and ended on November 8 to cover the intensive field campaign, and the first week was discarded as model spin-up time.

Emissions data were prepared as follows. Anthropogenic emissions were obtained from the Regional Emission inventory in ASia (REAS) version 2.1 (Kurokawa *et al.*, 2013); however, the latest year covered is 2008. There is no anthropogenic emission inventory during the intensive field campaign; therefore, we prepared the anthropogenic SO_2 emissions as follows. For China, which is the largest SO_2 emitter in East Asia, the satellite-based SO_2 column variation over China was used to evaluate the emissions variation. The SO_2 column observed by the Ozone Monitoring Instrument captured a declining trend after 2011 over the North China Plain area (i.e., Hebei and Shanxi provinces) (Krotkov *et al.*, 2016); hence, this decrease ratio was used to create the tentative SO_2 emissions amounts for China in 2015. From the variation of SO_2 column over Chinese provinces (van der A *et al.*, 2017), the decreasing trend over the North China Plain area can be a proxy of that over whole China; because this area is one of a dominant source of anthropogenic SO_2 emissions in China. This decrease ratio is mainly driven by the power plant sector (e.g., Wang *et al.*, 2015); however, we adjusted the amount of SO_2 emissions because the emission source categories were not the focus of this study. For other countries in East Asia, national-scale emissions estimations were adjusted for Taiwan (TWEPA, 2016), Korea (NIER, 2016), and Japan (JATOP, 2012a, b) based on the target year 2010. The spatial allocations were assumed to be the same as REAS. For other regions in the modeling domain, SO_2 emissions were not adjusted. The anthropogenic SO_2 emissions distribution is shown in Fig. 1. Biogenic emissions were prepared from the Model of Emissions of Gases and Aerosols from Nature (MEGAN) (Guenther *et al.*, 2012). Biomass burning emissions were used from the REanalysis of the TROpospheric chemical composition (RETRO) climatological database (Schultz *et al.*, 2008). SO_2 emissions from volcanoes were taken from the ACE-Asia and TRACE-P Modeling and Emission Support System (Streets *et al.*, 2003). Fifteen main active volcanoes in Japan and Mt. Mayon in Luzon Island, Philippines were considered (Fig. 2). In Japan, the amount of SO_2 emissions from volcanic activity surpassed the amounts of anthropogenic emissions; hence, the amount of SO_2 was further modified by observation data on volcanic activity during the calculation period from the Japan Meteorological Agency (JMA, 2016). The SO_2 emission amounts used in this study are summarized in Table 1.

To estimate the sources of SO_4^{2-}, we used the Particulate Source Apportionment Technology (PSAT) method in CAMx (Wagstrom *et al.*, 2008). This method assigns tracers to track the sources; hence, we refer to this method as the tagged tracer method. The concentration of each tracer is tagged to the specified emission source groups (i.e., source region and category). When i (i = 1, …, N) indicates the emission source groups, the SO_2 and SO_4^{2-} tracers are

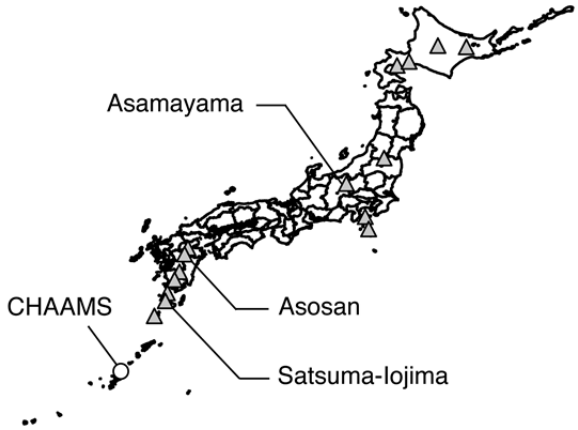

Fig. 2. Locations of the volcanoes for which the SO_2 emissions were considered. The three named volcanoes are those with the greatest activity (SO_2 emissions greater than 0.5 Gg day^{-1}) during October–November 2015.

Table 1. SO_2 emission amounts used in this study. Ship emissions are summarized over the whole model domain in this study.

	SO_2 emissions (Gg day^{-1})
Anthropogenic	
China	34.6
Taiwan	0.3
Korea	1.1
Japan	1.5
Ships	2.6
Volcanoes	
Asamayama	1.3
Asosan	0.9
Satsuma-Iojima	0.5
Others total	1.5

denoted as SO_{2i} and $SO_4^{2-}{}_i$, respectively. Based on the mass consistency between the modeled concentration (SO_4^{2-}) and the sum of the tracers' concentration ($\sum_{i=1}^{N} SO_4^{2-}{}_i$), the tracers' concentration can be used for source apportionment, which attributes the emission source groups, *i*. The temporal variations of the SO_4^{2-} tracers' concentration were determined according to the variation of SO_4^{2-} and the apportionment of tracers of $SO_4^{2-}{}_i$ during the transport and deposition processes; meanwhile, the SO_4^{2-} tracers were determined according to the variation of SO_4^{2-} and the apportionment of tracers of SO_{2i} during the production of SO_4^{2-}. The linear response in the production was assumed to transfer the information of emission source groups. The usefulness of the tagged tracer method for SO_4^{2-} over East Asia with respect to the validity of the linear assumption has been already reported (Itahashi *et al.*, 2017a). In this study, we prepared seven source groups: five sources for anthropogenic emissions from mainland China, Taiwan, the Korean Peninsula, Japan, and other regions in the modeling domain, including the lateral boundary condition; one source for ship emissions; and one source for volcano emissions as a natural source. In this work, the source region of Japan did not include Okinawa, where CHAAMS is located. Based on the REAS emission inventory, local anthropogenic SO_2 emissions from Okinawa were less than 1% of the total anthropogenic emissions from Japan; therefore, we regarded Okinawa as a remote site. The source apportionment for Japan represented LRT from mainland Japan.

RESULTS AND DISCUSSION

Model Evaluation

To evaluate the model reproducibility, the model results were compared with observations. Fig. 3 presents the observed and modeled meteorological field at CHAAMS. The temporal variation of wind speed (Fig. 3(a)) and direction

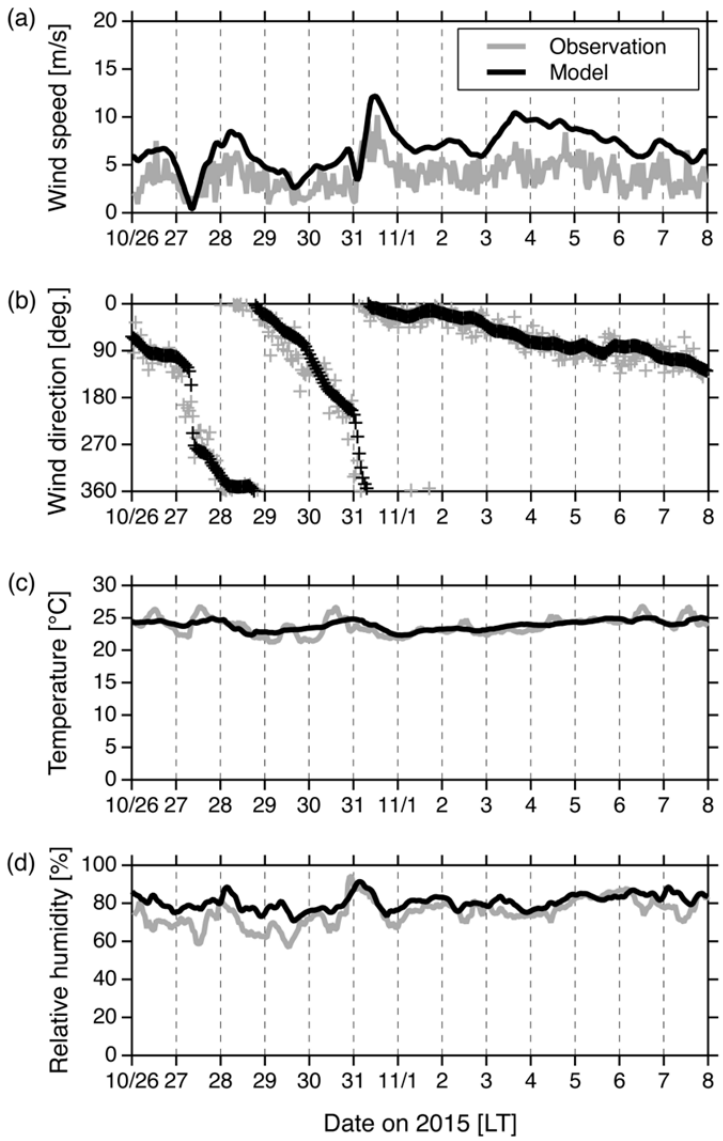

Fig. 3. Temporal variation of the meteorological fields of (a) wind speed, (b) wind direction, (c) temperature, and (d) relative humidity for observations (gray) and the model (black).

(Fig. 3(b)) were well captured by the model, although the wind speed was slightly overestimated. This was partly because CHAAMS was resolved as an ocean grid at the current model resolution. The wind direction was easterly on October 26, westerly on October 27–28, changed rapidly from northerly to southerly on October 29–30, and changed more slowly from northerly to easterly after October 31 until the end of the study period. The temperature was 20–25°C during the campaign and the model captured the variation, although the modeled variation range was smaller than the observed variation (Fig. 3(c)). During the period, precipitation higher than 1 mm h^{-1} was only observed at 21:00 LT, October 30 with 25.7 mm h^{-1}. During this precipitation event, the model greatly underestimated the amount of rainfall as 7.4 mm h^{-1} with a 3 h delay (data not shown). At the nearest JMA meteorological observation site of Oku within 5 km of CHAAMS, precipitation was 2.5 mm h^{-1} at 21:00 LT and 10.5 mm h^{-1} at 22:00 LT on October 30; the observed precipitation was a local event and was difficult for the model to capture. Relative humidity was around 80% during the campaign with a maximum of around 95%, which corresponded to the precipitation event. The model tended to overestimate the observation before this event, although it captured the observed variation well afterward (Fig. 3(d)).

The model SO_4^{2-} concentrations were compared with those obtained by the two observation methods. The results from the high-volume air sampler for $PM_{2.5}$ and the cascade impactor with six segregated size bins were compared with the model results (Figs. 4(a) and 4(b)). For the cascade impactor, the concentration of particles with D_p of less than 2.5 µm (corresponding to $PM_{2.5}$) was summed. During the period, the averaged SO_4^{2-} concentration was around 3.0 µg m^{-3} for both the observations and the model; the model captured the observed concentrations with a good correlation ($R > 0.8$). From the statistical analysis, the mean fractional bias and mean fractional error were calculated and were within the performance goal criteria proposed by Boylan and Russel (2006). High concentrations greater than 4.0 µg m^{-3} were observed on October 27 and November 1 and 3 with both observation methods, and they were also observed on November 4 by the high-volume sampler and on October 31 by the cascade impactor. In Fig. 4, each symbol is colored according to the model conversion ratio (*Fs*) from SO_2 to SO_4^{2-}, which is calculated from the molar concentrations

$$Fs = \frac{SO_4^{2-}}{SO_2 + SO_4^{2-}} \tag{2}$$

This ratio represents the fraction of precursor gases of SO_2 and secondary aerosols of SO_4^{2-}. A ratio of 0% indicates no production of SO_4^{2-}, and that of 100% indicates the complete conversion of SO_2 to SO_4^{2-}. Assuming that the local SO_2 emissions at CHAAMS are negligible, *Fs* was used as the index of the LRT impact to identify whether the air mass was fresh (lower *Fs*) or aged (higher *Fs*). During the episode, *Fs* varied from under 70% to over 95%. For the intensive observation on January 2015 at Fukuoka (33.52°N, 130.47°E) in western Japan, the model estimated that *Fs* was 30% for transboundary air pollution from China (Itahashi *et al.*, 2017b). This result suggested that SO_4^{2-} concentration at CHAAMS was affected by an aged air mass during the period. The event on November 1 showed the lowest *Fs* value of 67.0% and the event on November 4 showed the highest *Fs* value of 97.3%. The variation of *Fs* during the high concentration of SO_4^{2-} at CHAAMS suggested the event was dominated by different types of aged air mass that may have originated from different sources. Hereafter, we discuss the estimated sources of SO_4^{2-} at CHAAMS by using the tagged tracer method considering the *Fs* variation.

Estimation of Source Apportionment of SO_4^{2-} at CHAAMS

The modeled SO_4^{2-} concentration, source

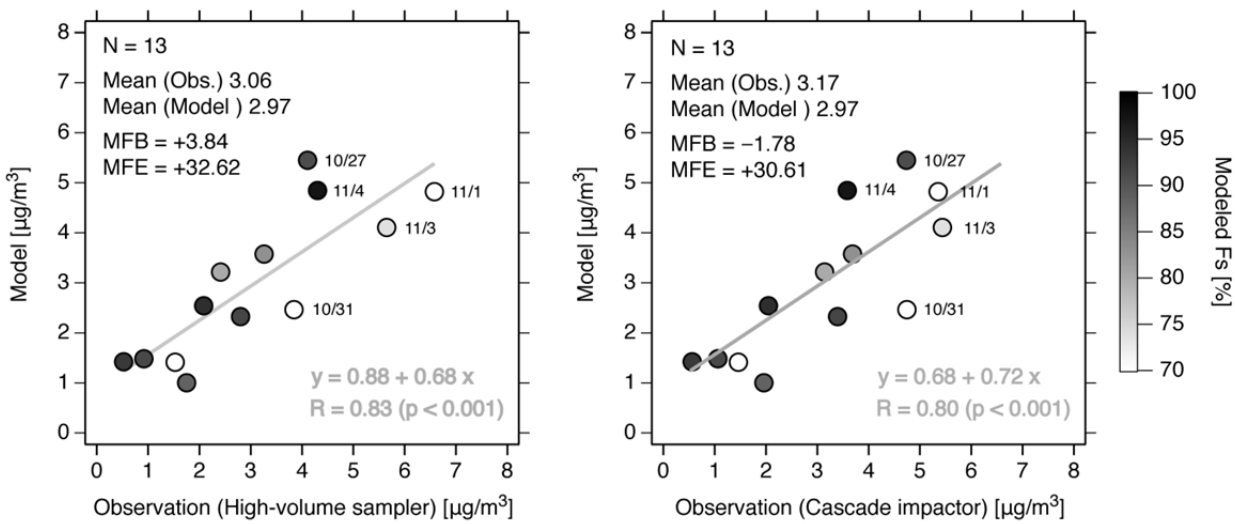

Fig. 4. Scatter plot of SO_4^{2-} concentration from the (left) high-volume sampler and (right) cascade impactor observations and the model. Color denotes the modeled *Fs*. Statistical analyses are shown in the inset.

apportionments by the tagged tracer method, and *Fs* values calculated with Eq. (2) at CHAAMS during the episode were averaged to give a daily value (Fig. 5). The results of source apportionments are shown as relative percentages to the modeled concentration and colored according to the source groups of anthropogenic emissions from mainland China, Taiwan, the Korean Peninsula, Japan, other regions, and ship emissions, and natural emissions from volcanoes. The source apportionment for China was continuously found during the observation campaign, but it was especially dominant on October 27 and 28, with the relative source apportionments of around 70%. These results were consistent with the westerly wind (Fig. 3(b)). Subsequently, source apportionments varied from day to day. On November 1, when *Fs* reached its lowest value, volcanoes were the largest source, with a relative source apportionment of 66.8%. On this peak day, the wind direction was mostly northerly (Fig. 3(b)), bringing an air mass from volcanoes in Japan to CHAAMS. After November 1, northerly to easterly winds continued, and volcanoes were identified as an important source of SO_4^{2-} at CHAAMS. On November 4, when *Fs* reached its highest value, the absolute source apportionments of Japan, Korea, and ships were the largest.

By averaging the source apportionment over the intensive observation campaign, the impact of volcanoes was the largest (40.8%), followed by China (34.3%), ships (8.7%), others (7.5%), the Korean Peninsula (4.6%), and Japan (4.2%). The source apportionment of Taiwan was less than 0.1% throughout the period. Fig. 5 shows that the sources of SO_4^{2-} at CHAAMS varied day-to-day during the period, so hereafter, we focus on the three high concentration events featuring *Fs* variation on October 27 and November 1 and 4.

Impact of China at CHAAMS

The maximum absolute source apportionment of China of 3.46 μg m^{-3} was revealed on October 27. To examine this event, the modeled spatial distribution of SO_4^{2-} and the source apportionments of mainland China, the Korean Peninsula, Japan, ships, and volcanoes are shown for October 27 in Fig. 6. The modeled high SO_4^{2-} concentration extended from mainland China to the East China Sea and reached to CHAAMS with a northwesterly wind (Figs. 6(a) and 3(b)). As a result, the source apportionment of China was dominant for this peak (Fig. 6(b)). In this event, *Fs* was relatively high at 90.8%. Because CHAAMS was over 650 km from Shanghai, the air mass from China was regarded as aged during the LRT. The Fs value of each tracer (SO_{2i} and $SO_4^{2-}{}_i$, where *i* denotes the emission source groups) was calculated with Eq. (2) (Table 2). During this event, the air mass that originated from China was highly aged with an *Fs* value of 95.8%. A similar dominant effect from China was previously reported based on aerial observations over East China Sea during spring (Hatakeyama *et al.*, 1997, 2011).

Impact of Volcanoes at CHAAMS

On November 1 (Fig. 7), the maximum absolute source apportionment of volcanoes was found to be 3.22 μg m^{-3}. This event was also characterized by the lowest value of *Fs* of 67.0%. The spatial distribution is shown in Fig. 7. A narrow air mass stream with a high concentration of SO_4^{2-} from western Japan (Kyushu Island) to eastern Taiwan was found (Fig. 7(a)), accompanied by a northerly wind (Fig. 3(b)). Because of the prevailing northerly wind over the East China Sea, the impact of China was limited to southern China (Fig. 7(a)). The narrow flow consisted of the volcano source apportionment (Fig. 7(f)). Kyushu Island has many volcanoes (7 of the 15 volcanoes considered in the modeling system), and these volcanoes, especially Asosan, which was active during the study period (Table 1), were responsible for the high concentration of SO_4^{2-} at CHAAMS. Table 2 shows the *Fs* values of each tracer, and the *Fs* value of 63.0% suggested that the air mass from volcanoes was relatively fresh. This was related to the fast transport over a higher altitude because of the injection height of volcanoes. A higher surface wind faster than 10 m s^{-1} was also found on October 31.

As an index of volcano source, coarse-mode SO_4^{2-} is related; as a counter-ion of volcanic ejecta (e.g., Ca). In addition, LeGrande *et al.* (2016) reported that during a volcano eruption the H_2O and SO_2 concentrations were

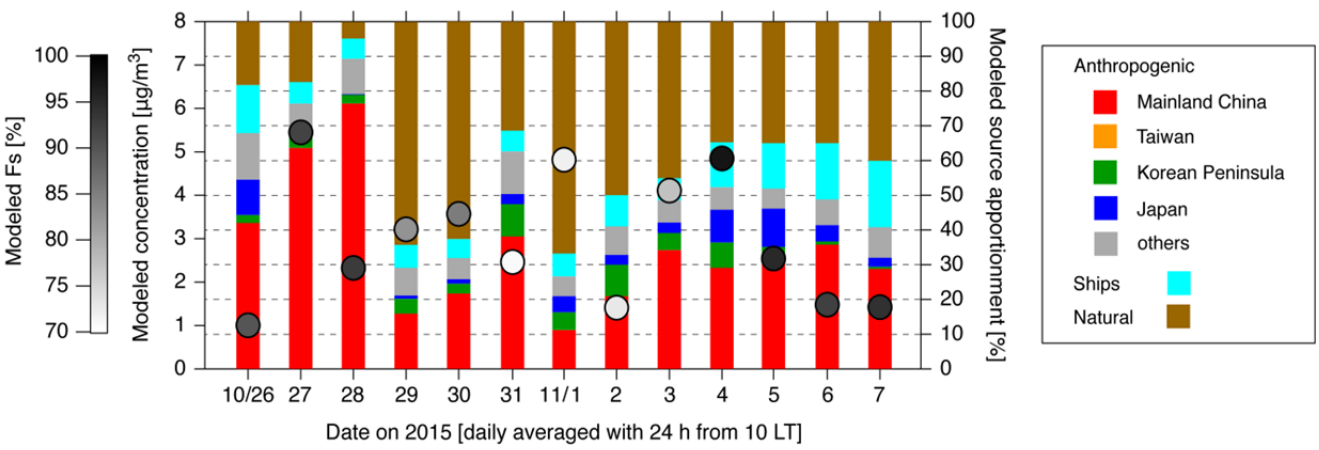

Fig. 5. Temporal variation of (left axis) modeled SO_4^{2-} concentration (grayscale circles indicate modeled *Fs*) and (right) stacked bar chart of source apportionment.

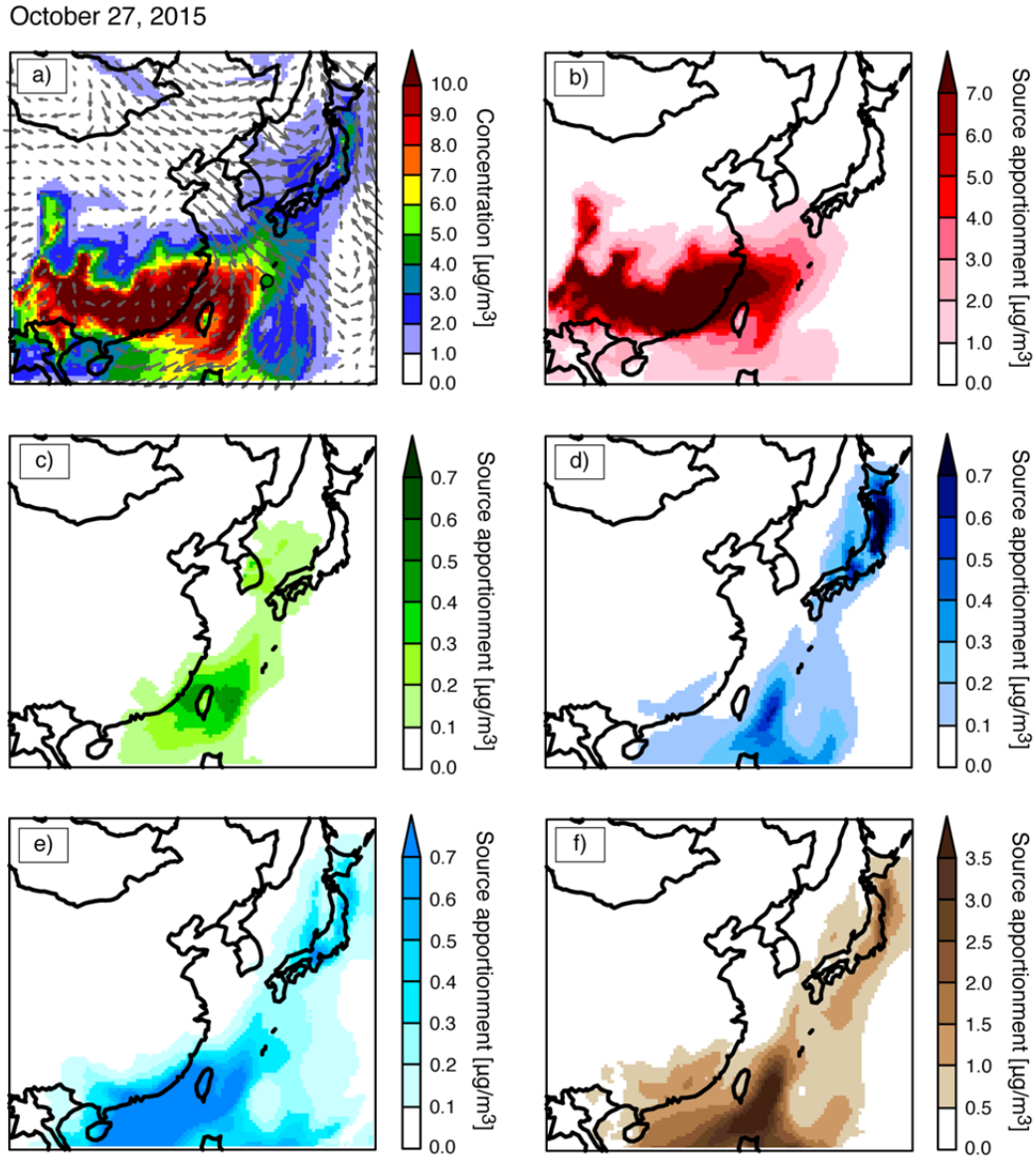

Fig. 6. Special distribution of (a) modeled SO_4^{2-} concentration, and source apportionment of (b) mainland China, (c) Korean Peninsula, (d) Japan, (e) ships, and (f) volcanoes on October 27.

Table 2. Modeled SO_4^{2-} concentration and *Fs* during high-concentration events on October 27, and November 1 and 4.

	October 27		November 1		November 4	
	SO_4^{2-} (μg m^{-3})	*Fs* (%)	SO_4^{2-} (μg m^{-3})	*Fs* (%)	SO_4^{2-} (μg m^{-3})	*Fs* (%)
Concentration	5.45	90.8	4.82	67.0	4.85	97.3
Source apportionment						
China	3.46	95.8	0.54	94.1	1.41	99.9
Korean Peninsula	0.17	99.5	0.25	83.2	0.35	99.3
Japan	0.15	99.8	0.22	73.3	0.45	98.7
Ships	0.34	64.9	0.32	53.3	0.63	86.3
Natural	0.95	99.8	3.22	63.0	1.69	98.9

high; a large amount of H_2O will promote SO_4^{2-} growth. Fig. 8 shows the temporal variation of the modeled volcano absolute source apportionment and coarse-mode SO_4^{2-} of D_p > 10 μm observed by the size-segregated cascade impactor. They showed moderate correlation (R = 0.64), and both revealed the maximum attribution to the volcano source on November 1. The approach of specifying emission sources both from model and observations is necessary to have confidence in the estimation results. Our results demonstrated an example of estimating the volcano source.

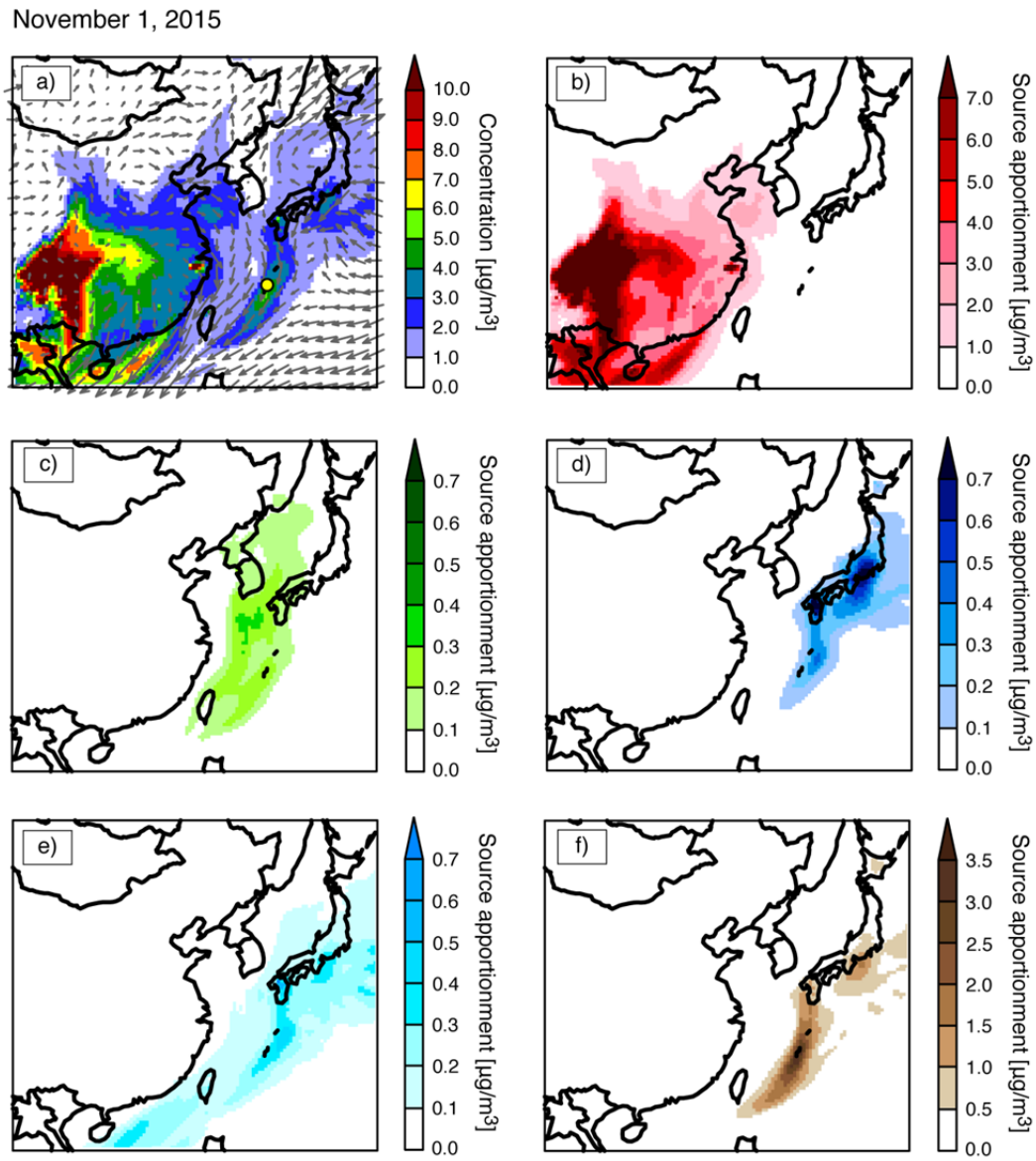

Fig. 7. Same as Fig. 6 but for November 1.

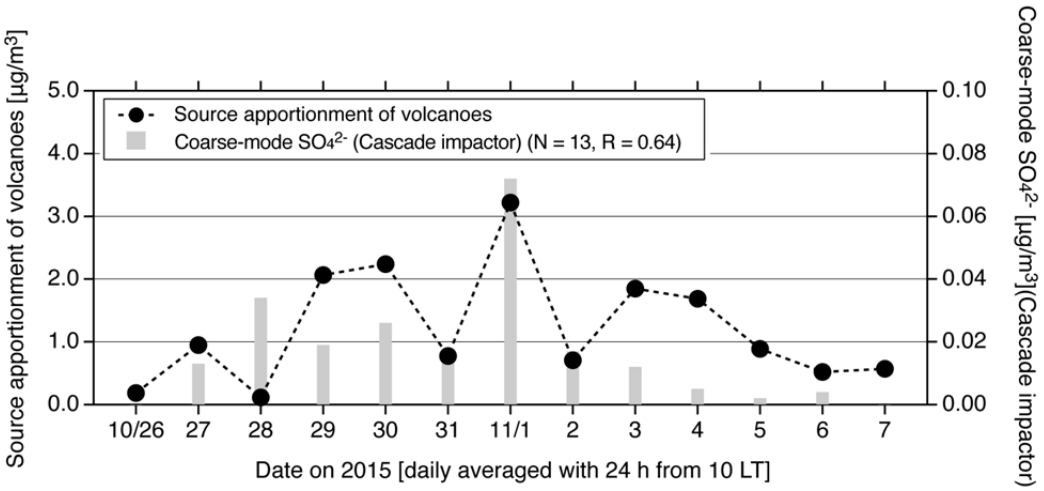

Fig. 8. Temporal variation of (left axis) modeled source apportionment of volcanoes (black circles with dotted lines) and (right) coarse-mode SO_4^{2-} observed by the cascade impactor (gray bar charts).

Impact of Ships at CHAAMS

On November 4 (Fig. 9), the high concentration of SO_4^{2-} that covered CHAAMS was affected by the easterly wind (Fig. 9(a)). From the spatial distribution of the modeled source apportionments, the contributions of Korea, Japan, and ships were determined for this event, and the maximum absolute source apportionments were 0.35, 0.45, and 0.63 μg m^{-3}, respectively, although they were smaller than those of China and volcanoes (Table 2). This event had a maximum value of *Fs* over 95%. The air mass from China, Korea, Japan, and volcanoes were highly aged with *Fs* over 98%. The air mass from ships had the highest *Fs* value of 86.3% for this event, compared with 64.9% and 53.3% for other two events (Table 2), and 50–70% during the whole period. Along the passage of the high-pressure system from eastern China (November 2, not shown) to South Korea (November 4, Fig. 9(a)), SO_4^{2-} was transported over a longer time by the easterly wind. This led to the aged air mass in the event on November 4.

The ship emissions source can be related to the observed V/Mn ratio (Hioki *et al.*, 2009; Shimada *et al.*, 2017). When an air mass is affected by oil combustion, the V/Mn ratio is increased because V is a tracer of oil combustion. In this comparison, two sets of V/Mn ratios were calculated from the high-volume air sampler and size-segregated cascade impactor. The size-segregated cascade impactor V/Mn values were calculated from the V concentration of $D_p < 0.1$ μm and Mn concentration of 2.5 μm < D_p < 10 μm. These diameter ranges were selected based on the analysis of crustal enrichment factors. It was confirmed that the V concentration of $D_p < 0.1$ μm indicated anthropogenic sources and the Mn concentration of 2.5 μm < D_p < 10 μm indicated natural sources. Fig. 10 shows the temporal variation of the modeled absolute source apportionment of ships and the observed V/Mn ratio. The high-volume air sampler results showed a good correlation (R = 0.53) and those for the cascade

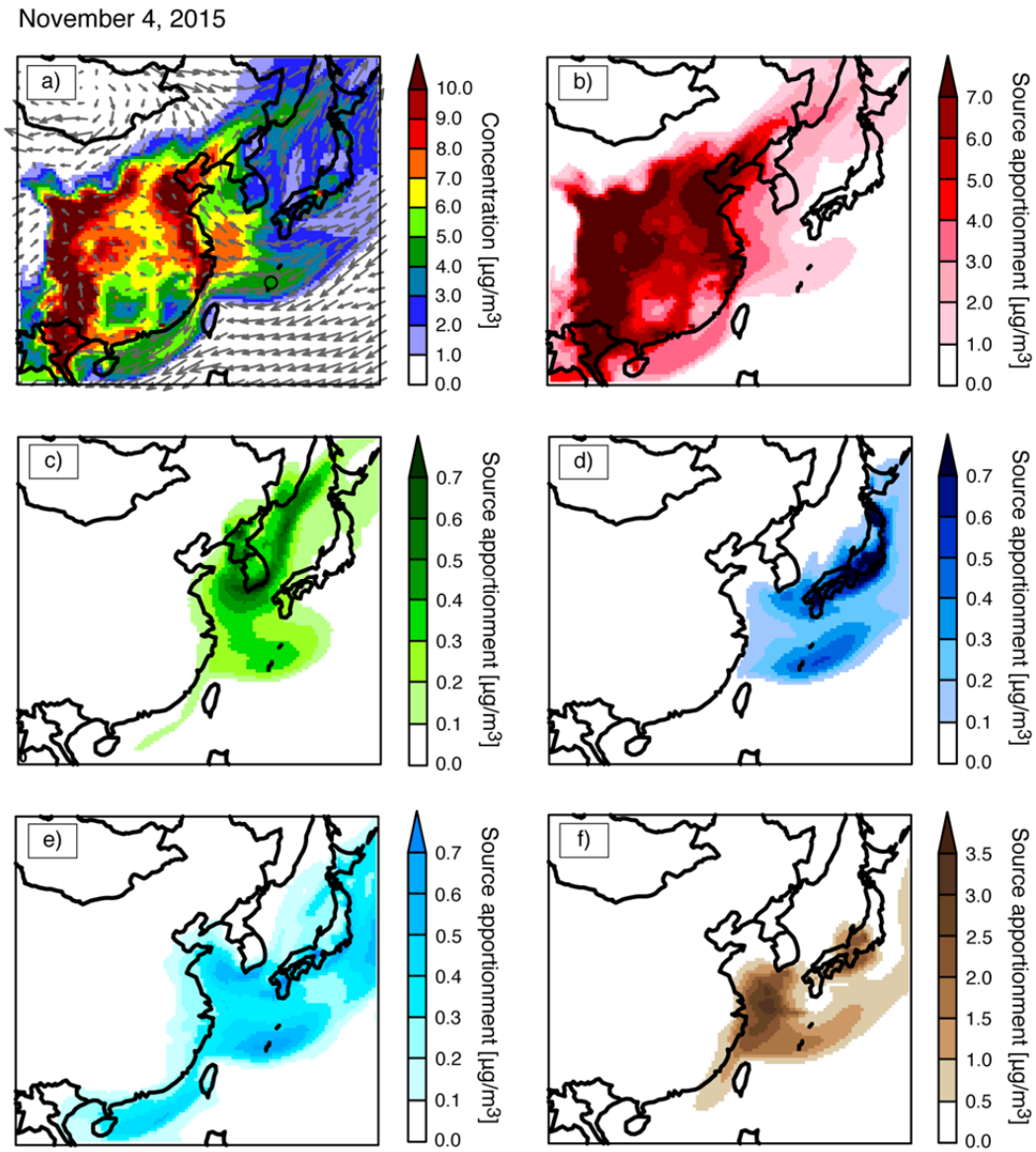

Fig. 9. Same as Fig. 6 but for November 4.

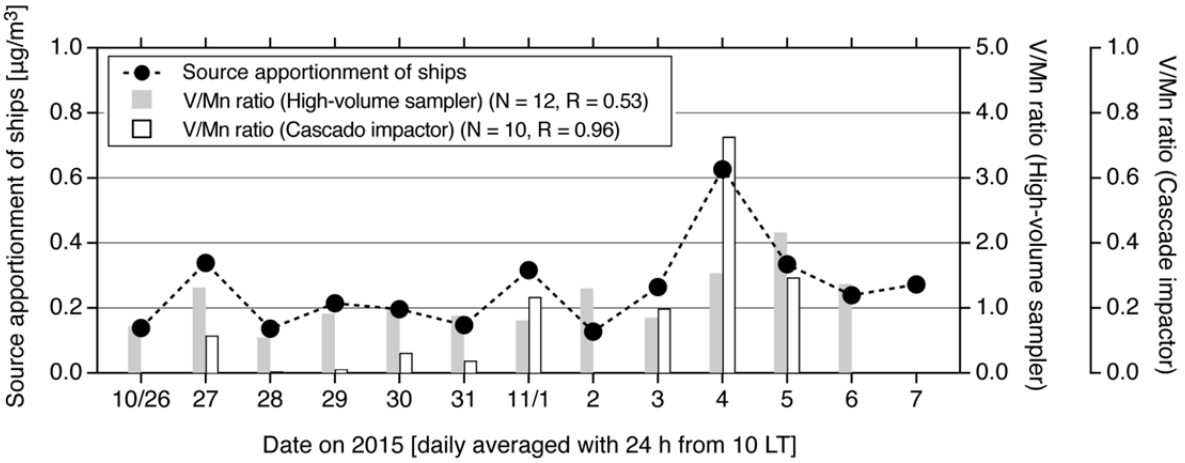

Fig. 10. Temporal variation of (left axis) modeled source apportionment of ships (black circles with dotted lines), and (right) V/Mn ratio observed by the high-volume air sampler (gray bar charts) and cascade impactor (white bar charts). Observation data from the high-volume air sampler on November 7, and from the cascade impactor on November 2, 6, and 7 were not calculated because of the detection limit of Mn.

impactor had a high correlation (R = 0.96) with the modeled source apportionment. The stronger effect of ships during the latter period suggested by both observations corresponded well to the model estimation. Additionally, the observed size-segregated V/Mn ratio indicated that the maximum contribution of the ship emission source on November 4 coincided with model estimation. Because the V/Mn ratio may contain information other than ship oil combustion, the V/Mn ratio based on the high-volume air sampler was higher on October 27 when the impact of China showed the largest contribution. Our results revealed that the size-segregated V/Mn ratio could be used as a ship source indicator to identify the effect of ship oil combustion. To the best of our knowledge, this is the first time that mutual source evaluation of ships has been performed by using the tagged tracer method with the chemical transport model and the observed V/Mn ratio. To improve our understanding of ship emission sources, more case studies should be performed.

CONCLUSIONS

Day-to-day variation of SO_4^{2-} sources at Cape Hedo, located on in the northernmost part of Okinawa, Japan (CHAAMS) was evaluated based on the air quality model with the tagged tracer method. The air quality model can capture the observed meteorological conditions and SO_4^{2-}. It was clarified that the high concentration episodes were affected by different sources. The air quality model with the tagged tracer method verified with the daily observation data identified and quantified a more detailed transport mechanism compared with our previous study (Itahashi *et al.*, 2017a), which was based on monthly or yearly averaged data.

On October 27, when the westerly wind was dominant, the absolute source apportionment of China was the highest. On November 1, when the northerly wind prevailed, the maximum source apportionment of volcanoes was observed, and was characterized by the lowest conversion ratio from SO_2 to SO_4^{2-} of less than 70%. During the latter part of campaign, northerly to easterly winds were prominent. The effects of Korea, Japan, and ships were also found, and these absolute source apportionments peaked on November 4. Because of the LRT, this event was characterized by the well-aged air mass with a conversion ratio of greater than 95%. For further confirmation of the source estimation results, the modeled source effects of volcanoes and ships were paired with the observed coarse-mode SO_4^{2-} and V/Mn ratio, respectively, and these pairs corresponded well. Based on the modeling results and observations, sources can be estimated with greater confidence.

ACKNOWLEDGMENTS

This research was supported by the Global Environment Research Fund (5-1452 and 2-1403) from the Ministry of the Environment of Japan. The authors acknowledge using MOZART-4 data for the global chemical transport model (http://www.acom.ucar.edu/wrf-chem/mozart.html) for the lateral boundary condition. The authors also thank JMA and other institutions for performing SO_2 observations of Japanese volcanoes.

REFERENCES

Aikawa, M., Ohara, T., Hiraki, T., Oishi, O., Tsuji, A., Yamagami, M., Murano, K. and Mukai, H. (2010). Significant geographic gradients in particulate sulfate over Japan determined from multiple-site measurements and a chemical transport model: Impacts of transboundary pollution from the Asian continent. *Atmos. Environ.* 44: 381–391.

Boylan, J.W. and Russell, A.G. (2006). PM and light extinction model performance metrics, goals, and criteria for three-dimensional air quality models. *Atmos. Environ.* 40: 4946–4959.

Carmichael, G.R., Adhikary, B., D'Allura, A., Tang, Y., Streets, D., Zhang, Q., Bond, T.C., Ramanathan, V., Jamroensan, A. and Marrapu, P. (2009). Asian aerosols: Current and year 2030 distributions and implications to human health and regional climate change. *Environ. Sci. Technol.* 43: 5811–5817.

Emmons, L.K., Walters, S., Hess, P.G., Lamarque, J.F., Pfister, G.G., Fillmore, D., Granier, C., Guenther, A., Kinnison, D., Laepple, T., Orlando, J., Tie, X., Tyndall, G., Wiedinmyer, C., Baughcum, S.L. and Kloster, S. (2010). Description and evaluation of the Model for Ozone and Related chemical Tracers, version 4 (MOZART-4). *Geosci. Model Dev.* 3: 43–67.

ENVIRON International Corporation (2014). *User's guide, comprehensive air quality model with extensions version 6.11*. ENVIRON International Corporation, Novato, CA, USA.

Guenther, A.B., Jiang, X., Heald, C.L., Sakulyanontvittaya, T., Duhl, T., Emmons, L.K. and Wang, X. (2012). The Model of Emissions of Gases and Aerosols from Nature version 2.1 (MEGAN2.1). An extended and updated framework for modeling biogenic emissions. *Geosci. Model Dev.* 5: 1471–1492.

Hatakeyama, S., Murano, K., Mukai, H., Sakamaki, F., Bandow, H., Watanabe, I., Yamato, M., Tanaka, S. and Akimoto, H. (1997). SO_2 and sulfate aerosols over the seas between Japan and the Asian continent. *Earozoru Kenkyu* 12: 91–95.

Hatakeyama, S., Hanaoka, S., Ikeda, K., Watanabe, I., Arakaki, T., Sadanaga, Y., Bandow, H., Kato, S., Kajii, Y., Sato, K., Shimizu, A. and Takami, A. (2011). Aerial observation of aerosols transported from East Asia chemical composition of aerosols and layered structure of an air mass over the East China Sea. *Aerosol Air Qual. Res.* 11: 497–507.

Itahashi, S., Uno, I, Yumimoto, K., Irie, H., Osada, K., Ogata, K., Fukushima, H., Wang, Z. and Ohara, T. (2012a). Interannual variation in the fine-mode MODIS aerosol optical depth and its relationship to the changes in sulfur dioxide emissions in China between 2000 and 2010. *Atmos. Chem. Phys.* 12: 2631–2640.

Itahashi, S., Uno, I. and Kim, ST. (2012b). Source contributions of sulfate aerosol over East Asia estimated by CMAQ-DDM. *Environ. Sci. Technol.* 46: 6733–6741.

Itahashi, S., Hayami, H. and Uno, I. (2015). Comprehensive study of emission source contributions for tropospheric ozone formation over East Asia. *J. Geophys. Res.* 120: 331–358.

Itahashi, S., Hayami, H., Yumimoto, K. and Uno, I. (2017a). Chinese province-scale source apportionments for sulfate aerosol in 2005 evaluated by the tagged tracer method. *Environ. Pollut.* 220: 1366–1375.

Itahashi, S., Uno, I., Osada, K., Kamiguchi, Y., Yamamoto, S., Tamura, K., Wang, Z., Kurosaki, Y. and Kanaya, Y. (2017b). Nitrate transboundary heavy pollution over East Asia in winter. *Atmos. Chem. Phys.* 17: 3823–3843.

Janssens-Maenhout, G., Crippa, M., Guizzardi, F., Dentener, F., Muntean, M., Pouliot, G., Keating, T., Zhang, Q., Kurokawa, J., Wankmuller, R., Danier van der Gon, H., Kuenen, J.J.P., Kilmont, Z., Frost, G., Darras, S., Koffi, B. and Li, M. (2015). HTAP_v2.2: A mosaic of regional and global emission grid maps for 2008 and 2010 to study hemispheric transport of air pollution. *Atmos. Chem. Phys.* 15: 11411–11432.

Japan Auto-Oil Program (JATOP) (2012a). *Emission estimates from motor vehicles*, JPEC-2011AQ-02-06, Tokyo, Japan (in Japanese).

Japan Auto-Oil Program (JATOP) (2012b). *Emission estimates from sources other than motor vehicles*, JPEC-2011AQ-02-07, Tokyo, Japan (in Japanese).

Japan Meteorological Agency (JMA), http://www.data.jma.go.jp/svd/vois/data/tokyo/volcano.html, (in Japanese) Last Access: 1 December 2016.

Kaneyasu, N. (2010). Development of $PM_{2.5}$ impactor for the conventional high-volume air sampler. *J. Japan Soc. Atmos. Environ.* 45: 171–174 (in Japanese).

Kaneyasu, N., Yamamoto, S., Sato, K., Takami, A., Hayashi, M., Hara, K., Kawamoto, K., Okuda, T. and Hatakeyama, S. (2014). Impact of long-range transport of aerosols on the $PM_{2.5}$ composition at a major metropolitan area in the northern Kyushu area of Japan. *Atmos. Environ.* 97: 416–425.

Krotkov, N.A., McLinden, C.A., Li, C., Lamsal, L.N., Celarier, E.A., Marchenko, S.V., Swartz, W.H., Bucsela, E.J., Joiner, J., Duncan, B.N., Boersma, K.F., Veefkind, J.P., Levelt, P.F., Fioletov, V.E., Dickerson, R.R., He, H., Lu, Z. and Streets, D.G. (2016). Aura OMI observations of regional SO_2 and NO_2 pollution changes from 2005 to 2015. *Atmos. Chem. Phys.* 16: 4605–4629.

Kurokawa, J., Ohara, T., Morikawa, T., Hanayama, S., Janssens-Maenhout, G., Fukui, T., Kawashima, K. and Akimoto, H. (2013). Emissions of air pollutants and greenhouse gases over Asian regions during 2000–2008: Regional Emission inventory in ASia (REAS) version 2. *Atmos. Chem. Phys.* 13: 11019–11058.

LeGrande, A.N., Tsigaridis, K., and Bauer, S.E. (2016). Role of atmospheric chemistry in the climate impacts of stratospheric volcanic injections. *Nat. Geosci.* 9: 652–655.

Nakajima, T., Yoon, S., Ramanathan, V., Shi, G., Takemura, T., Higurashi, A., Takamura, T., Aoki, K., Sohn, B., Kim, S., Tsuruta, H., Sugimoto, N., Shimizu, A., Tanimoto, H., Sawa, Y., Lin, N., Lee, C., Goto, D. and Schutgens, N. (2007). Overview of the atmospheric brown cloud East Asian regional experiment 2005 and a study of the aerosol direct radiative forcing in East Asia. *J. Geophys. Res.* 112: D24S91.

National Institute of Environmental Research (NIER) National Air Pollutants Emission Service, http://airemiss.nier.go.kr/mbshome/mbs/airemiss/index.do, Last Access: 1 December 2016.

Schultz, M.G., Heil, A., Hoelzemann, J.J., Spessa, A., Thonicke, K., Goldammer, J.G., Held, A.C., Pereira, J.M.C. and van het Bolscher, M. (2008). Global wildland fire emissions from 1960 to 2000. *Global Biogeochem. Cycles* 22: GB2002.

Shimada, K., Shimada, M., Takami, A., Hasegawa, S., Fushimi, A., Arakaki, T., Izumi, W. and Hatakeyama, S. (2015). Mode and place of origin of carboneous aerosols

transported from East Asia to Cape Hedo, Okinawa, Japan. *Aerosol Air Qual. Res.* 15: 799–813.

Shimada, K., Araki, Y., Yoshino, A., Takami, A., Yang, X., Chen, X., Meng, F. and Hatakeyama, S. (2017). Concentrations of metallic elements in long-range-transported aerosols measured simultaneously at three coastal sites in China and Japan. *J. Atmos. Chem.*, *in Press*.

Skamarock, W.C., Klemp, J.B., Dudhia, J., Gill, D.D., Barker, D.M., Duda, M.G., Huang, X.Y., Wang, W. and Powers, J.G. (2008). *A description of the advanced research WRF version 3. NCAR Tech. Note, NCAR/TN-475+STR*. National Center for Atmospheric Research, Boulder, Colorado, USA, 113 pp.

Streets, D.G., Bond, T.C., Carmichael, G.R., Fernandes, S.D., Fu, Q., He, D., Klimont, Z., Nelson, S.M., Tsai, N.Y., Wang, M.Q., Woo, J.H. and Yarberl, K.F. (2003). An inventory of gaseous and primary aerosol emissions in Asia in the year 2000. *J. Geophys. Res.* 108: 8809.

Taiwan Environmental Protection Administration (TWEPA) (2015). Taiwan Emission Data System (TEDS), Version 8.1, http://teds.epa.gov.tw/new_main2-0-1.html.

Takami, A., Miyoshi, T., Shimono, A., Kaneyasu, N., Kato, S., Kajii, Y., and Hatakeyama, S. (2007). Transport of anthropogenic aerosols from Asia and subsequent chemical transformation. *J. Geophys. Res.* 112: D22S31.

Takiguchi, Y., Takami, A., Sadanaga, Y., Lun, X., Shimizu, A., Matsui, I., Sugimoto, N., Wang, W., Bandow, H., and Hatakeyama, S. (2008). Transport and transformation of total reactive nitrogen over the East China Sea. *J. Geophys. Res.* 113: D10306.

Taniguchi, Y., Shimada, K., Takami, A., Lin, N.H., Chan, C.K., Kim, Y.P. and Hatakeyama, S. (2017). Transboundary and local air pollutants in western Japan distinguished on the basis of ratios of metallic elements in size-segregated aerosols. *Aerosol Air Qual. Res., in Press*.

Tatsuta, S. Shimada, K., Chan, C.K., Kim, Y.P., Lin, N.H., Takami, A. and Hatakeyama, S. (2017). Contributions of long-range transported and locally emitted nitrate in size-segregated aerosols in Japan at Kyushu and Okinawa. *Aerosol Air Qual. Res.* 17: 3119–3127.

van der A, R.J., Mijling, B., Ding, J., Koukouli, M.E., Liu, F., Li, Q., Mao, H. and Theys, N. (2017). Cleaning up the air: Effectiveness of air quality policy for SO_2 and NO_x emissions in China. *Atmos. Chem. Phys*. 17: 1775–1789.

Wagstrom, K.M., Pandis, S.N., Yarwood, G., Wilson, G.M. and Morris, R.E. (2008). Development and application of a computationally efficient particulate matter apportionment algorithm in a three-dimensional chemical transport model. *Atmos. Environ.* 42: 5650–5659.

Wang, S., Zhang, Q., Martin, R.V., Philip, S., Liu, F., Li, M., Jiang, X., and He, K. (2015). Satellite measurements oversee China's sulfur dioxide emission reductions from coal-fired power plants. *Environ. Res. Lett.* 10: 114015.

Zhang, Q., Jimenez, J.L., Canagaratna, M.R., Allan, J.D., Coe, H, Ulbrich, I., Alfarra, M.R., Takami, A., Middlebrook, A.M, Sun, Y.L, Dzepina, K, Dunlea, E., Docherty, K., DeCarlo, P.F., Salcedo, D., Onasch, T., Jayne, J.T., Miyoshi, T., Shimono, A., Hatakeyama, S., Takegawa, N., Kondo, Y., Schneider, J., Drewnick, F., Borrmann, S., Weimer, S., Demerjian, K., Williams, P., Bower, K., Bahreini, R., Cottrell, L., Griffin, R.J., Rautiainen, J., Sun, J.Y., Zhang, Y.M. and Worsnop, D.R. (2007). Ubiquity and dominance of oxygenated species in organic aerosols in anthropogenically influenced Northern Hemisphere midlatitudes. *Geophys. Res. Lett.* 34: L13801.

Received for review, December 30, 2016
Revised, June 5, 2017
Accepted, June 13, 2017